Copyright © 2013 Scienceline Publication

Journal of Civil Engineering and Urbanism

Volume 3, Issue 6: 342-356 (2013) **ISSN-2252-0430**

The Hydraulics of Flow in Non-Prismatic Compound Channels

Hojjat Allah Yonesi[*1], Mohammad Hossein Omid[2], Seyed Ali Ayyoubzadeh[3]

[1]*Ph.D student of Hydraulic Structures, Department of Irrigation and Reclamation Engineering, Faculty of Agricultural Engineering and Technology, University of Tehran, Karaj, Iran*
[2]*Professor of Hydraulic Structures, Department of Irrigation and Reclamation Engineering, Faculty of Agricultural Engineering and Technology, University of Tehran, Karaj, Iran*
[3]*Associate Professor of Hydraulic Structures, Faculty of Agricultural, Tarbiat Modares University, Tehran, Iran*

*Corresponding author's Email address: yonesi_h@ut.ac.ir r

ABSTRACT: This paper investigates the effects of floodplains' roughness the on hydraulic overbank flow in compound channels with non-prismatic floodplains. Experiments are carried out using three divergence angles and three roughness sizes on the floodplain. The velocity was measured using a three dimensional acoustic Doppler velocimeter and directional current meter in a lattice along the divergence channel with different depth ratios. Velocity distributions on the half-width of the channels in three portion of the flume (entrance, middle and end of the divergence) were measured. Using the experimental data about the values of the shear stress, depth–averaged velocity, roughness coefficient, turbulence parameters and divided discharge between the main channel and floodplain, the water surface slope was evaluated. Also these results were compared with the prismatic compound channel and also compared using the Shiono-Knight method.

Keywords: Diverging compound channel, Roughness ratio, Angle of divergence.

ORIGINAL ARTICLE
Received 11 Sep. 2013
Accepted 03 Nov. 2013

Notation

ΔA_i	Sub section area
B	width of main channel
b	width of flood plain
D_r	Depth ratio, defined as floodplain depth (y_f)/main channel depth (H)
D_{50}	Mean of sediment size
d	Bed material size
f	Darcy-Weisbach friction factor
g	Gravitational acceleration
H	Flow depth in main channel
H_e	Energy Head
K	Ratio of the transverse V and longitudinal U depth-averaged velocity
k_s	Equivalent sand roughness
m	Water surface slope
n	Manning's roughness coefficient
NP	Non-Prismatic section
P	Prismatic section
Q	Discharge
Q_a	Actual discharge
Q_s	Summation discharge
Q_e	Relative error between actual discharge and SKM or M-SKM
q_{fp}	Flood plain discharge
R^2	Regression coefficient
R_e	Reynolds number
R_{e*}	Reynolds number related to shear velocity
S_e	Energy line slope
S_{0x}, S_{0y}	Longitudinal and transverse channel be slopes
U, V	Mean velocity in stream wise and lateral direction
U_d	Depth-averaged velocity
U_{di}	Depth-averaged velocity in each panel
U_{mc}	Mean velocity in main channel
U_{fp}	Mean velocity in flood plain
ΔU	Velocity difference between main channel and floodplain
u_z	Local velocity at depth=z
u_0	Elevation corresponding to zero velocity
u_*	Bed shear velocity
u'v',u'w',v'w'	Reynolds shear stress
x, y	Stream wise and lateral directionsrespectively
y_{fp}	Depth flow on flood plain
y_j, y_{j-1}	Distance between points j and j-1
z	Vertical position above the bed
Γ	Secondary flow term in SKM
λ	Dimensionless eddy viscosity coefficient
κ	Von Karman's constant
ρ	Water density
ν	Kinematic viscosity
τ_b	Local boundary shear stress
τ_j, τ_{j-1}	Shear stress value at section j and j-1
θ	Divergence angle
τ_{zx}	Reynolds stress in the z-directionon plane perpendicular to x direction
ξ	Roughness ratio
ψ	Shear stress ratio at lateral direction

Subscripts

fp	refer to flood plain
mc	refer to main channel
M	Modified method
J, J-1	distance between each point to before point

INTRODUCTION

The flow in a compound channel differs from that in a simple channel because by increasing the water level in the main channel and by entering flow over the floodplain's surface, a strong reaction between the main channel and the floodplain will be generated near the junction region, which is due to the velocity difference between the main channel and the floodplain. In such a situation, secondary flows are generated in the interface between the main channel and floodplain, which consume a lot of momentum in these regions. Until recently, many researchers have been working on hydraulics of prismatic sections such as distribution of boundary shear stress, shear force and present equations for apparent shear force and correlation between flow depth with velocity and discharge. (Knight and Demetriou 1983, Knight and Hamed 1983, Meyers, 1987).Generated secondary current in the compound channel was modelled by Shiono and Knight assuming a linear variation for velocity in the lateral direction (SKM) (Shiono and Knight, 1991).

Tominaga and Nezu (1991) investigated the 3-D turbulence structure in various bed roughnesses and channel geometry. Cao et al. (2006), using the FCF data, present a new formulation for the momentum flux and flow resistance in the compound channel. Using the Boussinesq assumption and the FCF data, investigate the dependence of the momentum transfer coefficient on ratio of floodplain width to the main channel width (b/B) and depth ratio ($Dr=y_{fp}/H$) which is the floodplain depth (y_{fp}) to the main channel depth (H)(Cao Z, Meng J, Pender G and Wallis S, 2006). Tang and Knight (2009) presented an analytical solution to investigated three models in open channel flows (Tang X and Knight DW ,2009).

Most of these studies have focused on the stage-discharge relationship, distribution of the boundary shear stress, velocity distribution, apparent shear stress, turbulent characteristics, secondary currents, and momentum exchange in compound channels in steady and uniform flow conditions.

In natural rivers, due to changes in the cross-sectional area, the state of the flow may be changed from uniform to non-uniform. Under such conditions, the hydraulic analysis will be more complicated compared to simple uniform flow. This subject was investigated by Bousmar and Zech (2004, 2006), Proust et al. (2006), Bousmar et al. (2006), Proust et al. (2010), Rezaei and Knight (2009), and Rezaei and Knight (2011). Bousmar and Zech (2004) assuming a steady uniform flow, developed a lateral distribution model (LDM) and extended it for a non-uniform flow. They also used the SKM model to define the ratio K=V/U and developed an expression for non-prismatic sections. In addition, they suggested that the secondary term is separate into two parts: (1) a dispersion term in the uniform flow due to the helical secondary currents and (2) a transverse convection term corresponding to the mass transfer due to the non-prismaticity.

Bousmar et al. (2006) using experimental data, investigated the hydraulic of the flow in the compound channel with enlarging floodplains. The important results they obtained were the direction of momentum transfer from the main channel to the floodplains, the discharge of the floodplain lower than the actual discharge on a long distance, and a flow asymmetry for the larger discharges.

Proust et al. (2010), using the first law of thermodynamics, estimated the energy losses in straight, skewed, divergent, and convergent compound channels. Their results show that the slope of energy line equals the head loss gradient at the total cross-section, yet the gradient of head loss differs with slope of energy line in the main channel or the floodplain.

Rezaei and Knight (2009) developed the SKM for compound channels with non-prismatic floodplains. Substituting the energy line slope (S_e) with the channel bed slope (S_{0x}), the convergence effects were accounted. This method was named the modified SKM.

Also, they (2011) studied on the hydraulics of the flow in a non-prismatic compound channel with different convergence angles. The results revealed that the velocity in the second half of the converging reach increased significantly.

All the above-mentioned studies have focused on the effect of changes in floodplain sections. The effect of roughness on the floodplain in non-prismatic compound channels has not been considered yet. This study then investigates the aforementioned effects in a non-prismatic compound channel by using the experimental data of a compound channel with three different divergence angles and three roughness ratios. Also, in this research, the results were compared with the SKM and modified SKM according to the results obtained by Rezaie and Knight (2009).

MATERIALS AND METHODS

Set-up

In this research, the experiments were performed in a symmetrical concrete compound channel flume with 15m long, 1.2 m wide with a flow recirculation system at the University of Tehran, Iran. The bed slope in the main channel and floodplain was $S_{0x}=0.88\times10^{-3}$. The cross-section was built with two flood plains(0.4m wide) and a main channel with 0.4 m wide (Figure1).

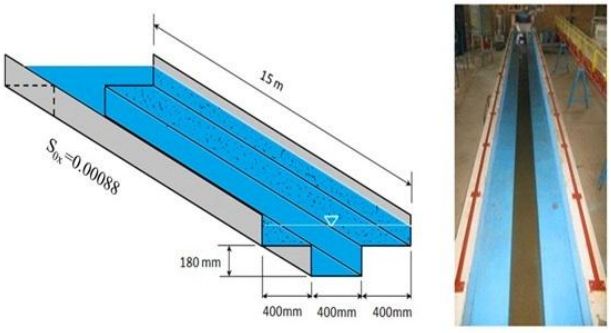

Figure 1. (a),(b) Details of prismatic compound channel

The depth of the main channel is 18 cm because the use of the Acoustic Doppler Velocimeter (ADV) to measure the velocity had a limitation of the water height on the floodplain (about 5 cm). The bed and the wall of the main channel were covered with uniform sediments with $D_{50}=0.65$ mm. The wall and surface of the floodplain were covered with sediments $D_{50}=0.65$, 1.3,

1.78 mm for different experiments. Two sets of experiments were performed as follow:

Experiments of the prismatic compound channel

In this condition, with three values of roughness on the floodplain and three-depth ratios, the experiments in the prismatic cross-section were performed. To achieve a uniform flow in each depth ratio, the flow depth (H) was adjusted using the downstream tailgate. Figure 2 depicts the values of the discharge versus head (Q-H) for different values of the roughness ratio (ξ) in the prismatic compound channel at above the bank full level. Then, based on the depth ratio, experimental discharges were selected for prismatic compound channels. Using the curve-fitting method, the following equations were proposed for the stage-discharge:

$$\xi = 1 \quad : \quad H = -18.86Q^2 + 4.872Q + 0.046 \qquad R^2 = 0.996$$
$$\xi = 2 \quad : \quad H = -2.747Q^2 + 3.902Q + 0.063 \qquad R^2 = 0.996$$
$$\xi = 2.74 \quad : \quad H = -18.44Q^2 + 5.955Q + 0.016 \qquad R^2 = 0.997$$

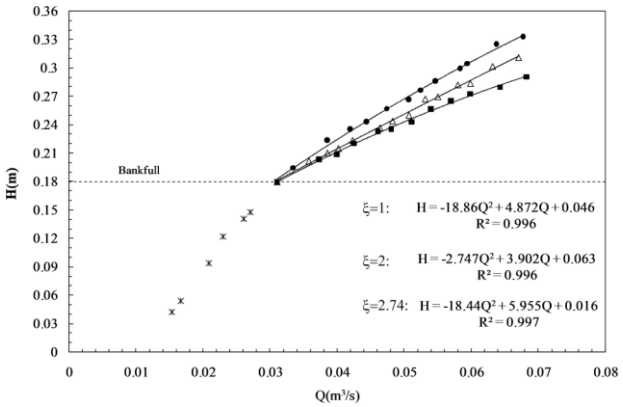

Figure 2. Stage-discharge curves in prismatic compound channel.

The actual discharge (Q_a) was adjusted using the triangular weir which was installed upstream of the flume and the discharges were compared with the discharges (Q_s) obtained from the summation of the depth-averaged velocities (U_{di}) per panel's area (Figure 3) as follows: $Q_s = \sum_{i=1}^{10} \Delta A_i . U_{di}$

In the above equation, ΔA_i is the panel's area and U_{di} is the depth-averaged velocity in each panel. Based on the experimental data, the percentage relative difference between the Q_a and Q_s was less than 4%.

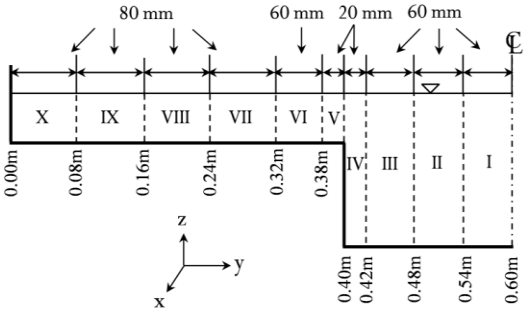

Figure 3. Schematic description of compound channel and section measurements velocity

For each experiment, the water surface elevation along the flume was recorded by a point gauge with the accuracy 0.1 mm. The velocity distributions were measured using a current meter with a 14 mm diameter in D_r=0.15, 0.25 and an ADV in D_r=0.35. The sampling frequency of ADV was 100 Hz and time of sampling was 60 seconds.

Non-Prismatic compound channel

In this non-prismatic shape, two Plexiglas walls about 5m of the upstream were isolated as a single channel and then three angles of divergence (3.8, 5.7 and 11.3 degree) in each run were constructed (Figure 4). Three values of roughness on the floodplain and three depth ratios were selected. The values of the discharge in the non-prismatic compound channel were similar to the ones of the experiments of the prismatic shape. The flow depth (H) was fixed at the middle of divergence area by adjusting the tailgate.

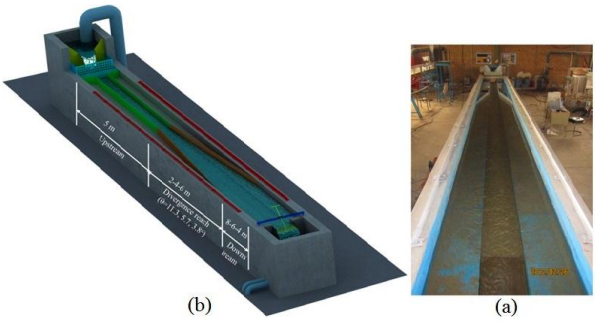

Figure 4. (a) Schematic 3-D of non-prismatic compound channel (θ =3.8°). (b) The view of non-prismatic compound channel (θ =11.3°)

In this research, two codes P-ξ-D_r and NP-θ-ξ-D_r were used to explain the experiments. Note that P and NP stand for prismatic and non-prismatic compound channels, respectively, θ is the angle of divergence, roughness ratio, ξ is defined as D_{50fp}/D_{50mc}, and D_r is the depth ratio. To obtain the data, the flow cross section was divided into suitable vertical (5~20 mm) and lateral distances as shown in Figure 3.In this research, the experimental data showed that the flow characteristics at both sides of the centre line of the compound channel were the same (Figure5). Thus sampling was made only for half of the total cross-section. The zonal discharge is calculated based on the depth-averaged velocity in each section and then the ratio of divided discharge between the main channel and floodplains in three regions was estimated.

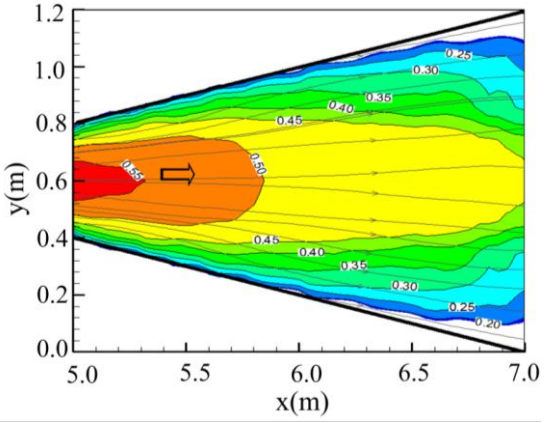

Figure 5. Symmetrical the velocity field in 190 mm above main channel bed in test NP-3.8-1-0.35

Both the velocity distribution and water surface elevation were measured as the same prismatic cross-section. Water surface elevations were measured along the centre of the flume at the intervals of 20cm in the divergence portion and 50 cm in other regions.

The values of the velocity were recorded in three sections: the entrance, middle, and end of the divergence reach. The characteristics of the experiments are summarized in Table 1.

Table 1. Summary of Experimental characteristics

Series	Floodplain Roughness Ratio(ξ)	Q_{actual} (lit/s)	Dr	Diverging angle (θ^0)	Froude Number	Reynolds Number×10^5	No. Of Experiments
P-ξ-Dr	1	41,50,61.5	0.15,0.25,0.35	-	0.198-0.254	0.874-1.295	9
	2	39,46.5,57	0.15,0.25,0.35	-	0.167-0.245	0.976-1.095	
	2.74	37,44,52	0.15,0.25,0.35	-	0.167-0.232	0.947-1.094	
NP-θ -1-Dr	1	41,50,61.5	0.15,0.25,0.35	3.8	0.252-0.293	1.478-1.984	9
				5.7			
				11.3			
NP-θ -2-Dr	2	39,46.5,57	0.15,0.25,0.35	3.8	0.236-0.284	1.407-1.822	9
				5.7			
				11.3			
NP-θ -2.74-Dr	2.74	37,44,52	0.15,0.25,0.35	3.8	0.212-0.263	1.334-1.697	9
				5.7			
				11.3			

In all of the experiments, the equivalent sand roughness (k_s) was greater than 2.2 mm, so the bed of the main channel and floodplain were rough ($k_s.u_*/\nu>70$) where ν is kinematic viscosity. The bed shear velocity was evaluated by using the stream wise mean velocity profiles conventional logarithm formula in all of the experiments in the rage of $0<z/H\leq0.2$ (Smart, 1999).

$$\frac{u_z}{u_*}=\frac{1}{\kappa}\ln(\frac{z}{z_0})$$

in which κ = Von Karman's constant(approximately equal to 0.4) z is the vertical distance above the bed, and z_0 is elevation corresponding to zero velocity($u_{z=z0}=0$) based on the data given by Nikuradse, $z_0$for $R_{e*}>70$ is 0.0331 k_s. Thus

$$\frac{u_z}{u_*}=5.75\log(\frac{30.2z}{k_s})$$

k_s may be calculated from the following relationship (Ackers,1991).

$$k_s=\left(8.25\sqrt{g}\,n\right)^6$$

That: Manning's coefficient (n) was calculated using strikler equation $(n=d_{50}^{\frac{1}{6}}/21.1)$. These values for three roughnesses equal 0.0139, 0.0157 and 0.0165, respectively. After calculating the bed shear velocity in all of the tests, the bed shear stress ($\tau=\rho u_*^2$) was calculated. The changes ratio of the shear stress in the lateral direction was defined as below:

$$\psi=\frac{\partial\tau}{\partial y}=\frac{\tau_j-\tau_{j-1}}{y_j-y_{j-1}}$$

in which τ_j, τ_{j-1} shear stress value in section j and j-1 respectively and y_j, y_{j-1} distance between points j and j-1.

Application of the SKM

Shiono and Knight developed an equation 2-D (SKM) by simplifying the Navier–Stokes momentum equation:

$$\rho gHS_{ox}+\frac{\partial}{\partial y}\left(\rho\lambda\sqrt{\frac{f}{8}}H^2U_d\frac{\partial U_d}{\partial y}\right)-\frac{\rho f}{8}\sqrt{1+S_{oy}^2}U_d{}^2=\Gamma$$

Where ρ = water density (kg/m^3), g =gravitational acceleration (m/s^2), H=flow depth in main channel (m), x, y=stream wise and lateral directions, respectively, S_{0x}=bed slope (m/m) in x direction, λ=dimensionless eddy viscosity coefficient, f=Darcy-Weisbach friction factor, U_d=depth-averaged velocity (m/s), S_{oy}=side wall slope (m/m), and Γ= Secondary flow term (N/m^2). In addition, some parameters are defined as:

$$U_d=\frac{1}{H}\int_{z=0}^{z=H}u\,dz\quad,\quad f=\frac{8\tau_b}{\rho U_d^2}$$

$$u_*=\sqrt{\frac{\tau_b}{\rho}}\quad,\quad\Gamma=\frac{\partial}{\partial y}[H(\rho VU)_d]$$

Where τ_b= local boundary shear stress (N/m^2), u_* = bed shear velocity (m/s), and U, V= velocity components (m/s) in the x, y directions, respectively.

The equation was presented for the steady and uniform flow at the prismatic compound channel. But in non-prismatic shape, the flow becomes non-uniform so that we could not use the bed slope. Rezaie and Knight (2009), substituting the energy line slope with the bed slope, considered the effects of non-uniformity of the flow in the SKM and named it modified SKM. In this research, we used this procedure in order to compare the results of this study with SKM, and modified SKM.

The model was used accordance with conditions imposed by Abril and Knight (2004) and Tang and

Knight too (2009). The details of the parameters used in the modelling SKM, and modified SKM have been shown in Table 2. A comparison between S_{ox} and S_e for NP-3.8-1-0.15 at five selected sections is shown in Figure 6.

Table 2. Parameters used in SKM and modified SKM to simulated in NP-11.3-1, 2, 2.74- 0.25

Test	n_c, n_f	f_1,f_3	λ_1, λ_3	Γ_1,Γ_3	α_2	γ_1,γ_3	S_0	S_e
NP-11.3-1-0.25	0.0139,0.0165	0.0335, 0.0918	0.07, 1.265	0.15, -0.25	1	6.41, 12.86	0.00088	0.000468
NP-11.3-2.74-0.25	0.0139,0.0165	0.0335, 0.0734	0.07, 0.604	0.15, -0.25	1	5.67, 9.38	0.00088	0.000571

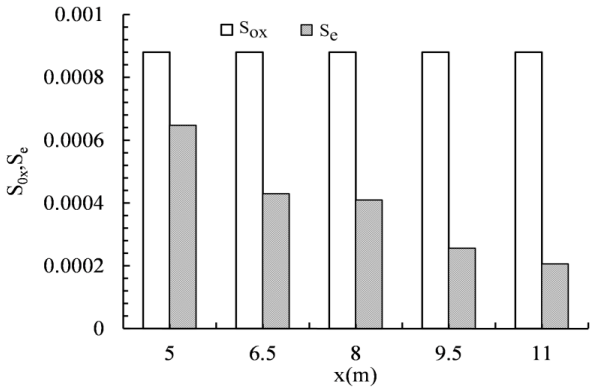

Figure 6. Comparison between bed slope S_{ox} and energy line slope S_e in NP-3.8-1-0.15

RESULTS AND DISCUSSION

Distribution of velocities

In the experiments, the local velocities were measured at nodes located in different depths and widths in each panel. In the prismatic channel velocity distribution in the longitudinal direction is shown in Figure 7 for the four tests P-1-0.15, P-2.74-0.15, P-1-0.35, and P-2.74-0.35.

The vertical distributions of the velocity with the logarithmic law are shown in Figure 9 for NP-11.3-1, 2.74-0.35 tests in two sections (middle and end of divergence reach).In all of the sections, the vertical velocity distributions obey the logarithmic distribution law, except for the near the interface zone.

Also in the main channel, the maximum velocity did not happen at the flow surface but at the floodplain, the maximum velocity was still at the flow surface.

The results showed that in a prismatic shape, by increasing D_r, the velocity gradient at interface zone decreased. If the roughness ratio also increased on the floodplain, the velocity gradient at interface zone will be increased. In a non-prismatic shape, an increase in D_r results in a decrease in the velocity gradient at interface zone. In all of the tests, the velocity gradient at the middle of divergence reach was much higher than the end of divergence reach.

In addition, by increasing the ξ or θ, these gradients increased. Based on equation 8, the parameter Γ had a direct relation with ξ and θ but an inverse relation with D_r.

Lateral depth-averaged velocity distributions were calculated and compared with the SKM and modified SKM in the tests of NP-11.3^o-ξ-0.25. The results are shown in Figure 10. As shown in this figure, in the non-prismatic compound channel with the same angle of divergence, increasing the roughness ratio or decreasing the depth ratio led to an increase in the difference between the mean velocity in the main channel and floodplain.

There is a good agreement between the results of the modified SKM and the experimental data. Although the accuracy of the modified SKM decreases, when the roughness ratio increases.

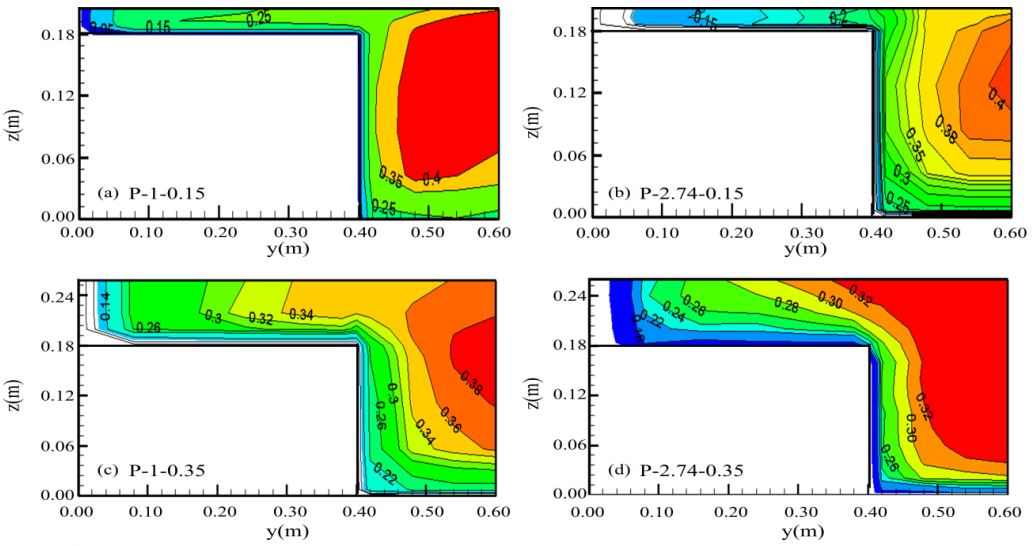

Figure 7. Velocity distribution (m/s) at (a, b) P-1, 2.74- 0.15 (c, d) P-1, 2.74- 0.35 respectively

In non-prismatic compound channel, velocity distributions were also shown in Figures 8 in two sections (the middle and end of divergence reach).

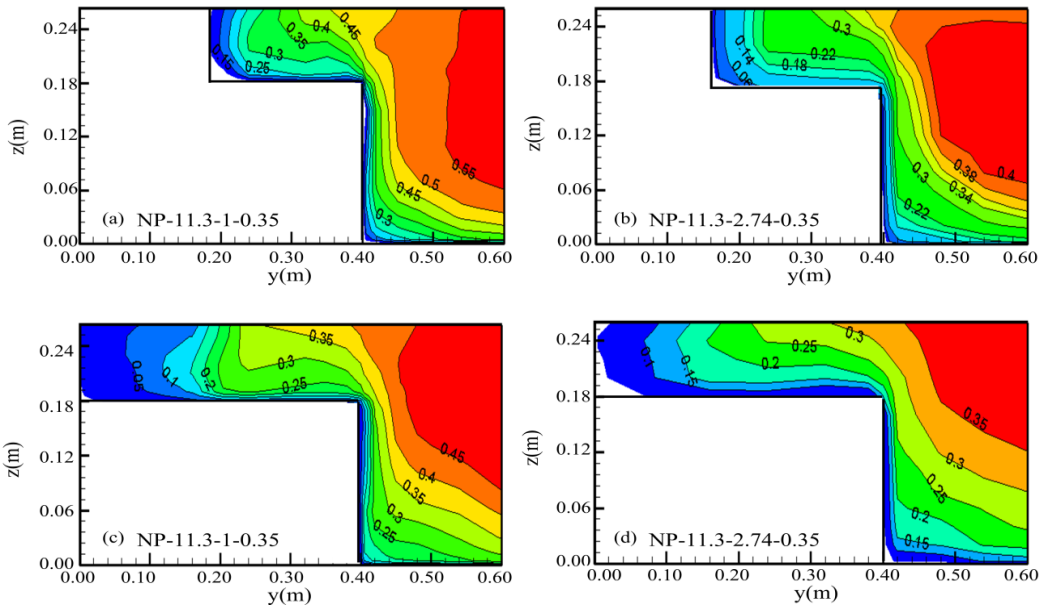

Figure 8. Velocity distribution (m/s) (a, b) middle (c, d) end of divergence reach in tests NP-11.3-1, 2.74-0.35 respectively

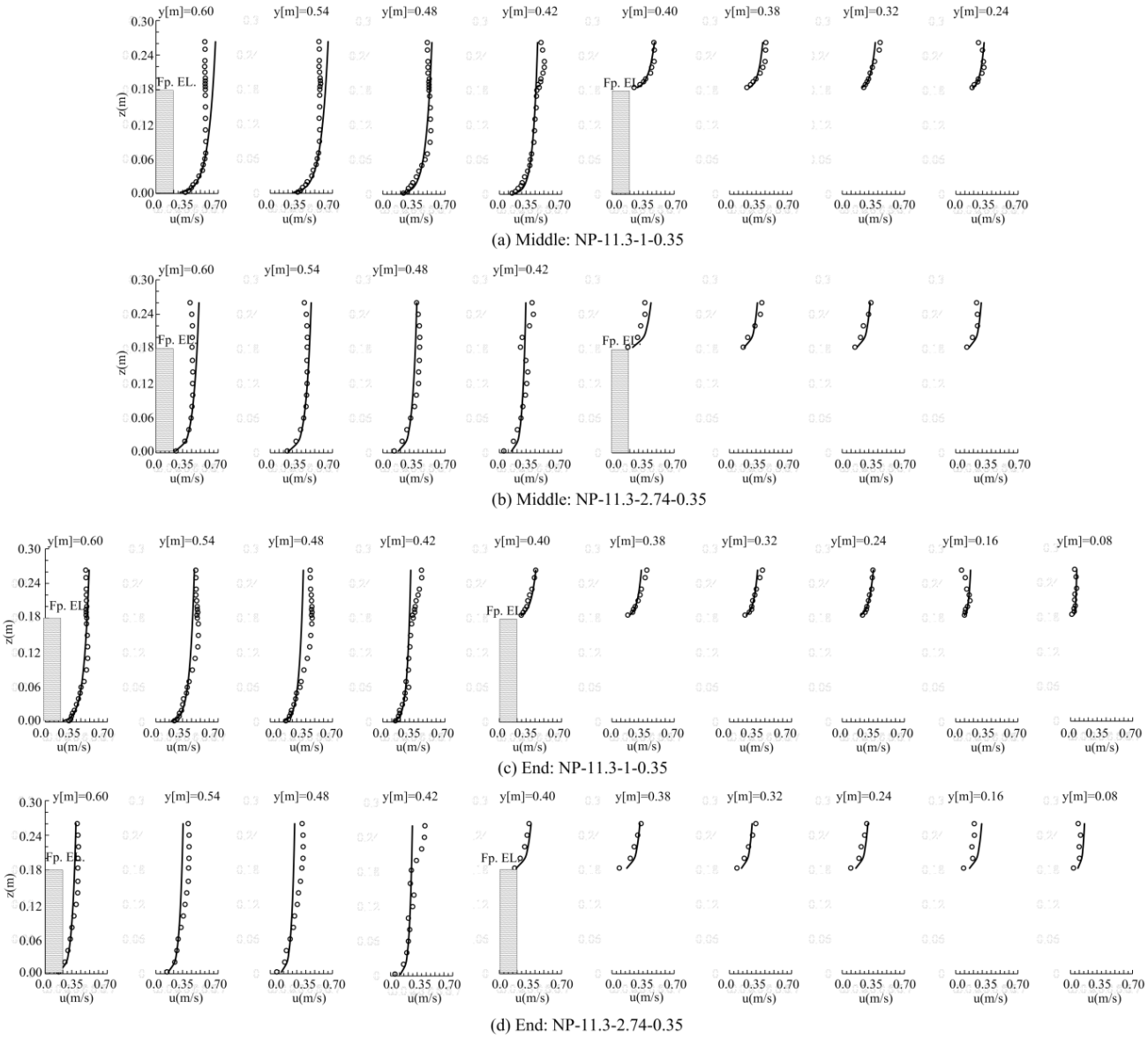

Figure 9. Comparison of vertical distribution of velocity data with logarithmic law at (a, b) middle (c, d) end of divergence reach in tests NP-11.3-1, 2.74-0.35 respectively

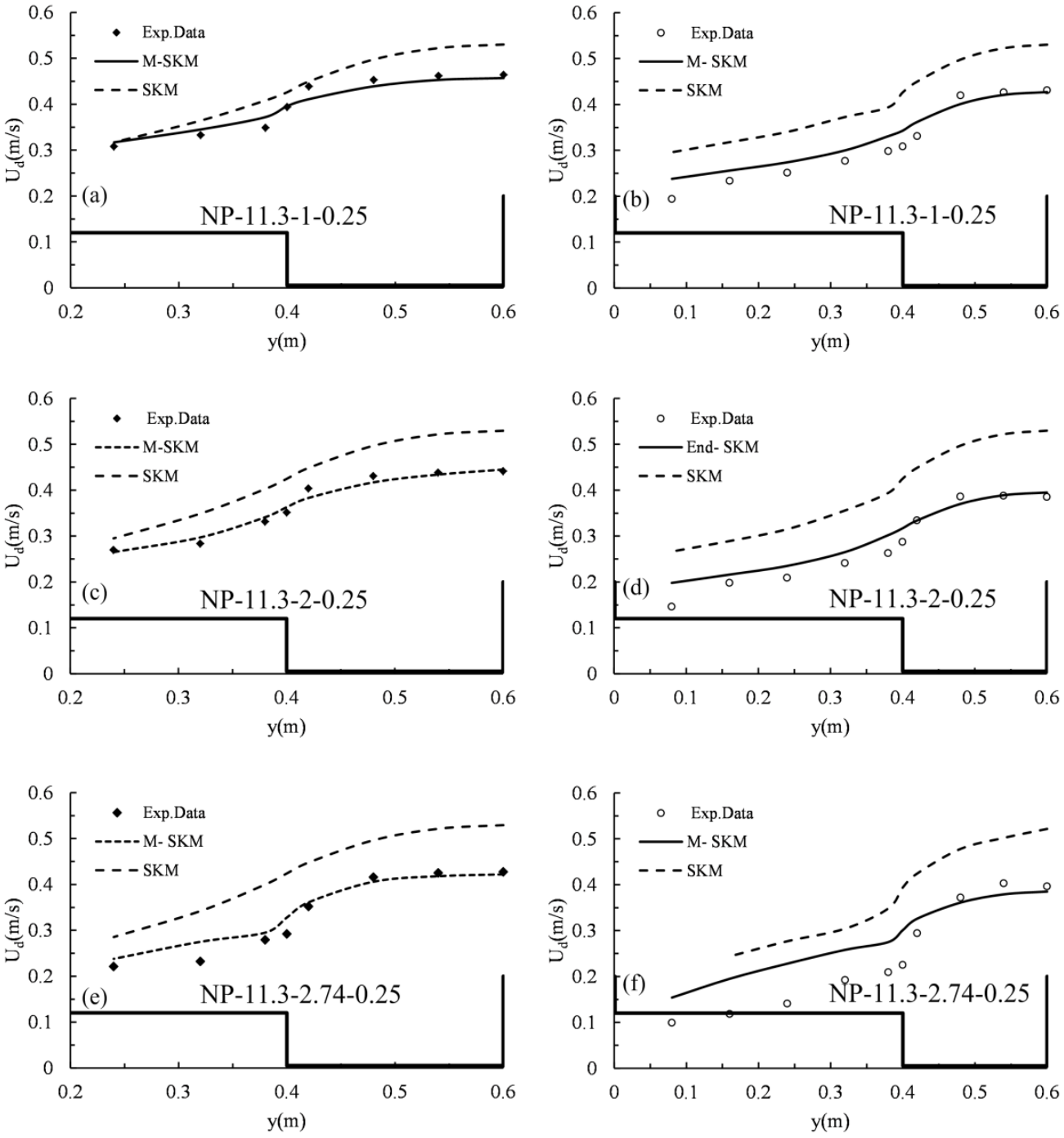

Figure 10. Comparison between lateral velocity distribution and results of modified SKM and SKM (a, b) NP-11.3-1-0.25 (c, d) NP-11.3-2-0.25 (e, f) NP-11.3-2.74-0.25

The ratio of the average velocity in the floodplain to main channel (U_{fp}/U_{mc}) for the prismatic shape (P-ξ-D_r) and non-prismatic compound channel in the tests NP-11.3^o-ξ-D_r were shown in Figure 11. Hu et al. (2010) report the same results. As shown in Figure 11, increasing the depth ratio (D_r) and decreasing roughness ratio (ξ), results in an increase in U_{fp}/U_{mc}. In addition, the value of U_{fp}/U_{mc} at middle of divergence area was a little more than the end of divergence reach. Myers et al. (1987) also reported this subject. These conditions were valid for all of the experiments. In the low depth ratio, the difference between the main channel velocity and floodplain was high. Therefore, the momentum transfer WAS much more than the high depth ratio.

The changes of local velocity components (u, v and w) and the Reynolds shear stress parameters in unit mass for prismatic and non-prismatic sections at middle of the divergence area near the interface were plotted. As shown in figure 12, at the middle of the divergence angle, the intensity of the velocity components and the Reynolds shear stress were much more than the prismatic section.

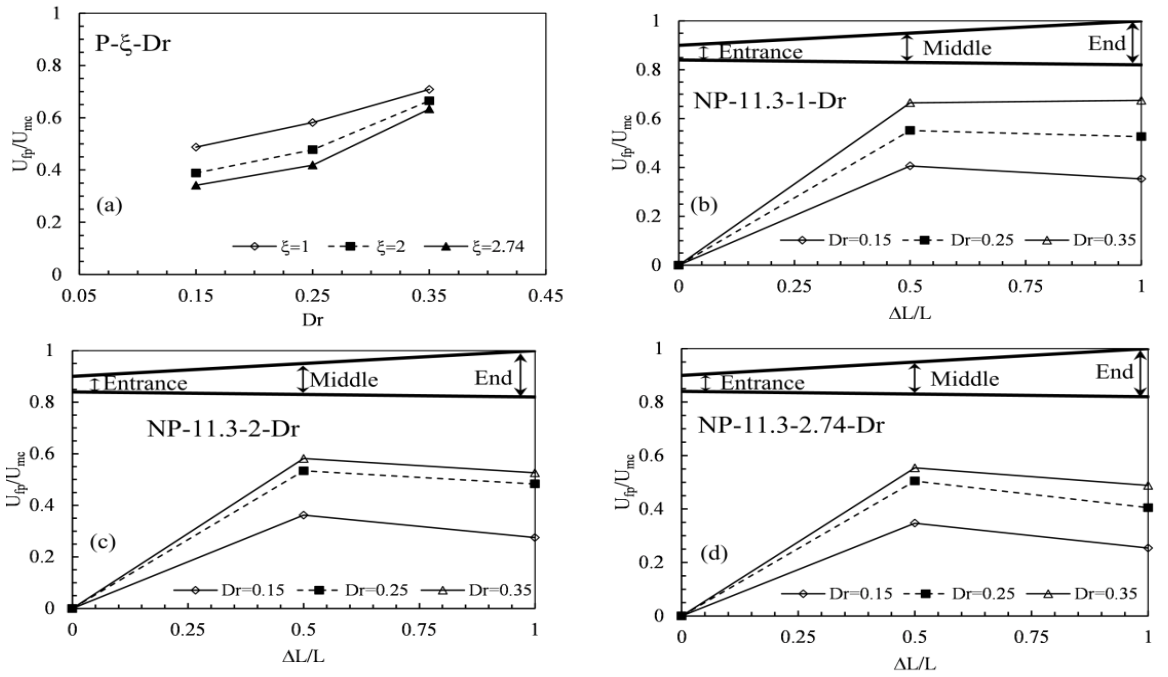

Figure 11. Average velocity ratio in floodplain to main channel (U_{fp}/U_{mc}) (a) P-ξ-D_r (b) NP-11.3-1-D_r (c) NP-11.3-2-D_r (d) NP-11.3-2.74-D_r

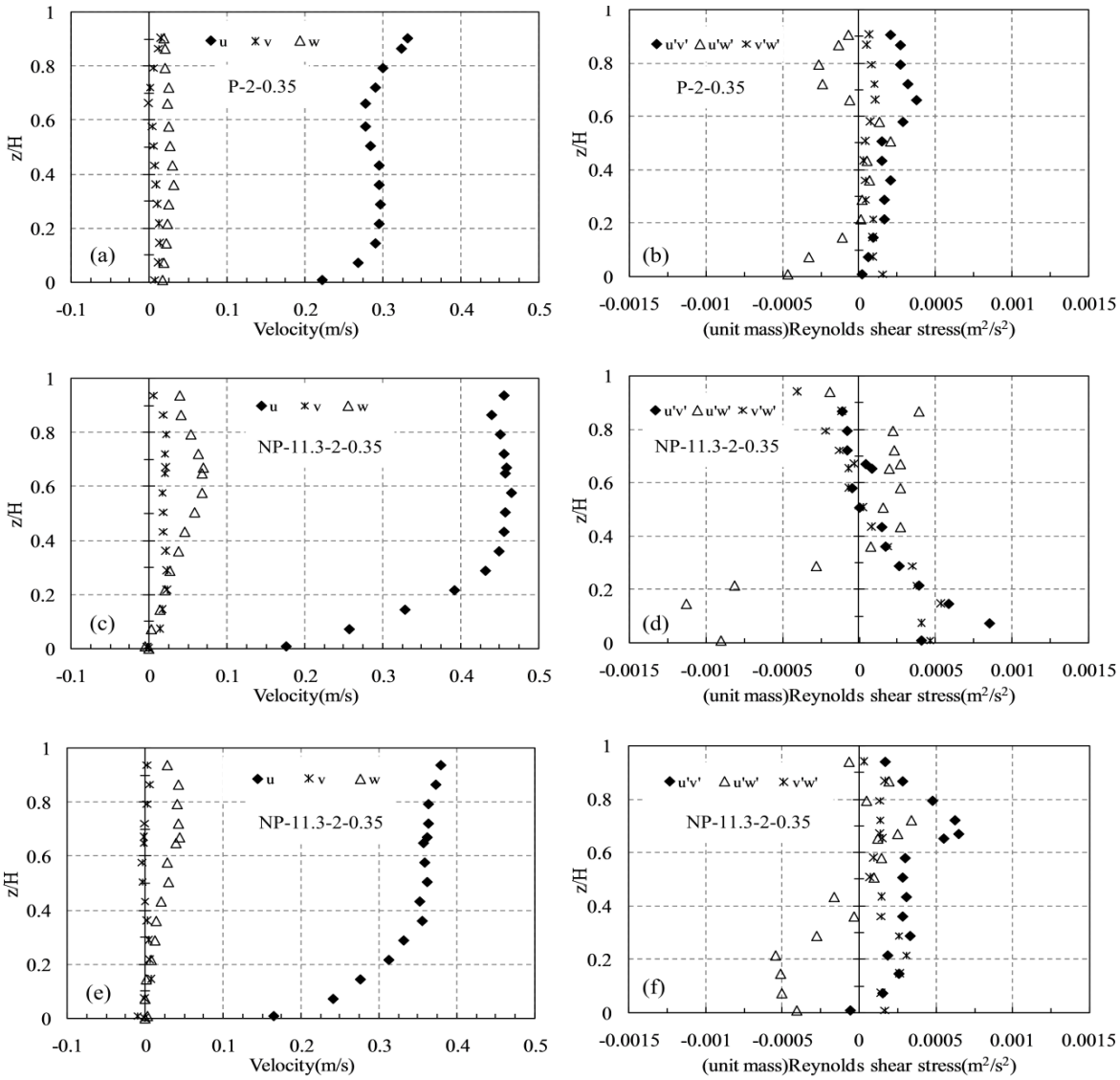

Figure 12. Local velocities and Reynolds shear stresses at y=405 mm (a, b) prismatic compound channel (P-2-0.35) (c, d) middle of divergence at main channel(NP-11.3-2-0.35) (e, f) end of divergence at main channel(NP-11.3-2-0.35)

Percentage divided discharge

The percentage-divided discharge was calculated by summation of the depth-averaged velocity (Equation 5) in the main channel and floodplains.

The percentage-divided discharge for different θ and ξ in the non-prismatic and prismatic section was shown in Figure 13. This figure shows that by increasing ξ, discharge portion on the floodplain decreased. Figure 14 shows the effect of increasing depth ratio on value of percentage-divided discharge. When the depth ratio increased, the floodplains had a greater share in carrying the discharge. This matter is also emphasized by Knight and Tang (2008).

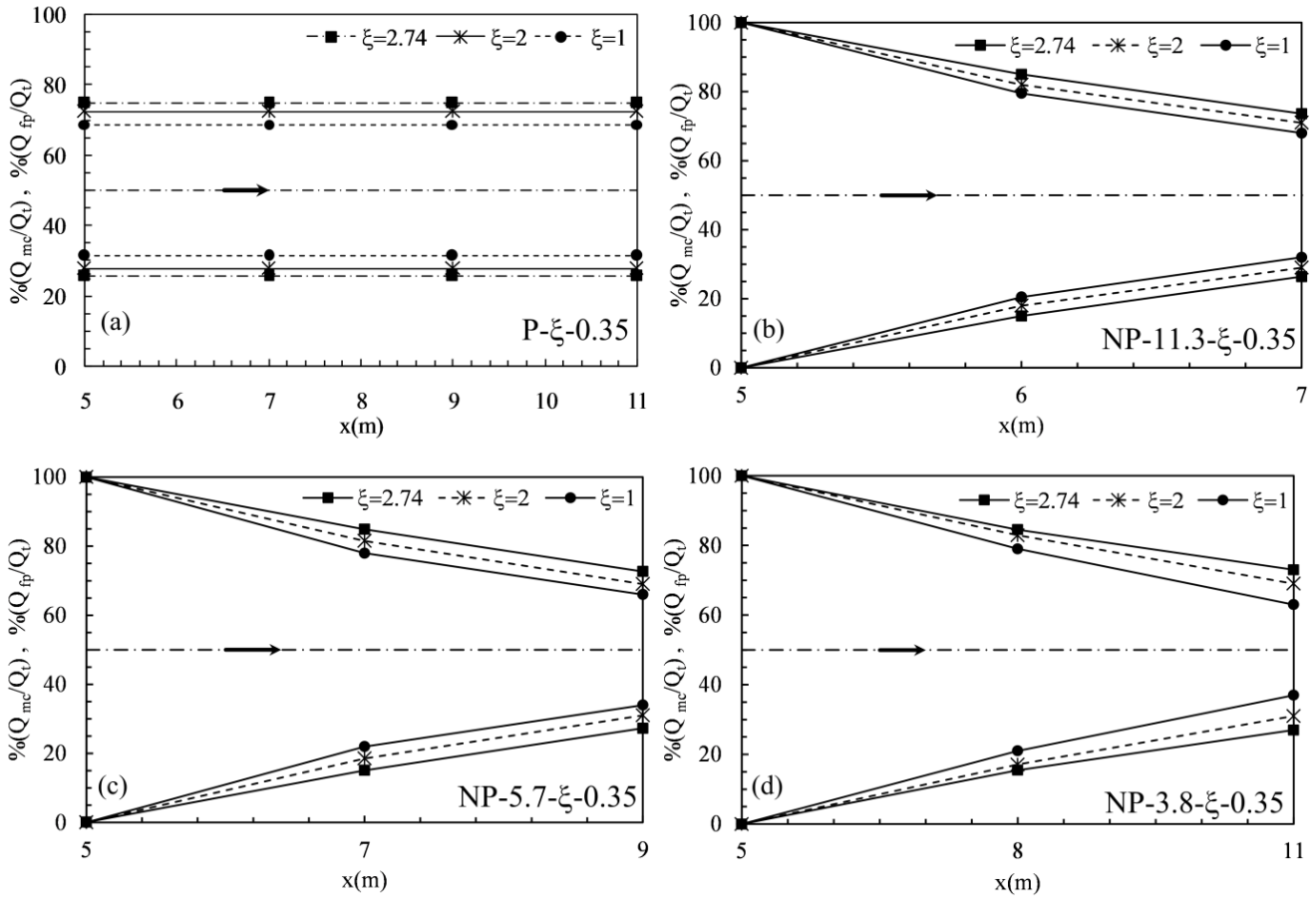

Figure 13. Determine the percentage divided discharge between the main channel and floodplain in (a) P-ξ-0.35 (b) NP-11.3-ξ-0.35 (c) NP-5.7-ξ-0.35 (d) NP-3.8-ξ-0.35.

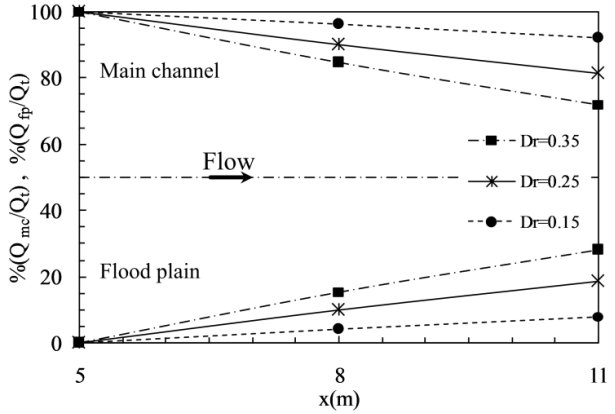

Figure 14. The effect of the depth ratio on percentage divided discharge between main channel and floodplain in NP-3.8- 2.74-D_r

In a non-prismatic section, the effect of the divergence angle was insignificant on the divided discharge, and only three parameters affected the divided discharge which was the velocity difference between the main channel and floodplain (ΔU), the flow depth on floodplain (y_f), and the roughness ratio (ξ).

Water surface slope and energy head

In experiments, the water surface elevation from upstream to downstream of the divergence was measured. The results show that an increase in the depth ratio and roughness ratio led to an increase in the slope of the water surface. This result holds for all the angles of divergence. Figure15 showed the results of NP-3.8°, 11.3° -ξ-0.15tests.

Using the curve fitting method, the water slope surface along divergence reach (m) was found as function of θ, ξ and D_r as:

$$m = 0.0057\frac{\xi^{0.17}}{(1-D_r)^{2.5}\theta^{0.08}} \qquad (R^2 = 0.959)$$

The changes of the water slope surface with the above parameters in the tests θ=3.8 and θ=11.3 are shown in Figure 16. In practical works, using ξ, D_r, θ, and the energy equation at the entrance of divergence reach, we can estimate the water level at end of this area. Then the head losses in this reach were calculated. Also we can estimate the discharge ratio between the main channel and floodplain.

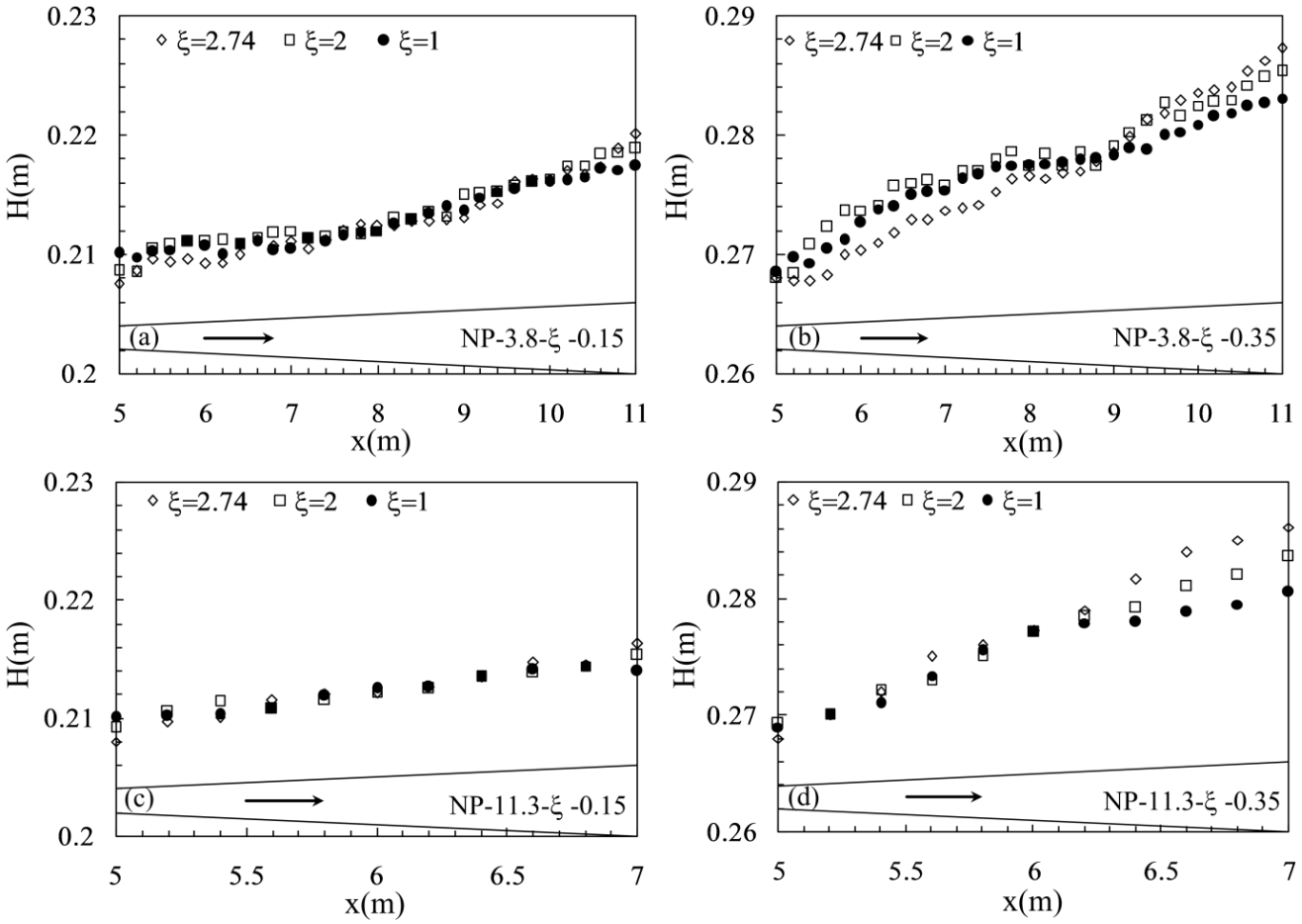

Figure 15. Changes of water surface elevation at divergence reach in (a, b) NP-3.8-ξ -0.15, 0.35 (c, d) NP-11.3-ξ -0.15, 0.35

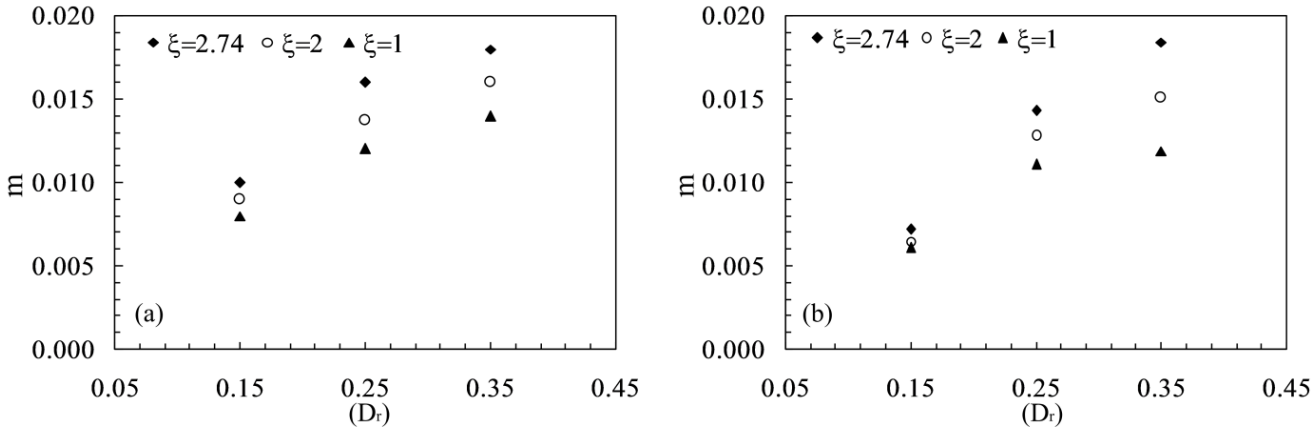

Figure 16. Water surface slope (m) in divergence reach with (a) θ=3.8° (b) θ=11.3°

By using the water surface profiles, the energy head (H_e) was calculated as follow:

$$H_e = Z_b + H + \alpha \frac{U^2}{2g}$$

The changes of water surface profile and energy head in test NP-3.8-2.74-0.25 along the centre of the main channel are shown in Figure 17.

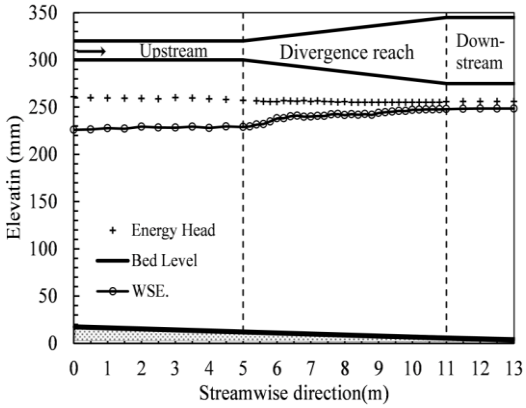

Figure 17. Water surface profile and energy head in NP-3.8-2.74-0.25

Friction factor

Using the following equation, the Darcy-Weisbach friction factor in each panel was calculated.

$$f = \frac{8\tau_b}{\rho U_d^2}$$

In Figure 18, the changes of the overall friction factor in the prismatic compound channel versus Reynolds number and flow depth values were plotted. In the prismatic section, equations were fitted through the data, as follows:

$$\xi = 1 \quad : \quad H = 0.793 f^{0.3952}$$
$$\xi = 2 \quad : \quad H = 0.689 f^{0.3603}$$
$$\xi = 2.74 \quad : \quad H = 0.631 f^{0.3451}$$

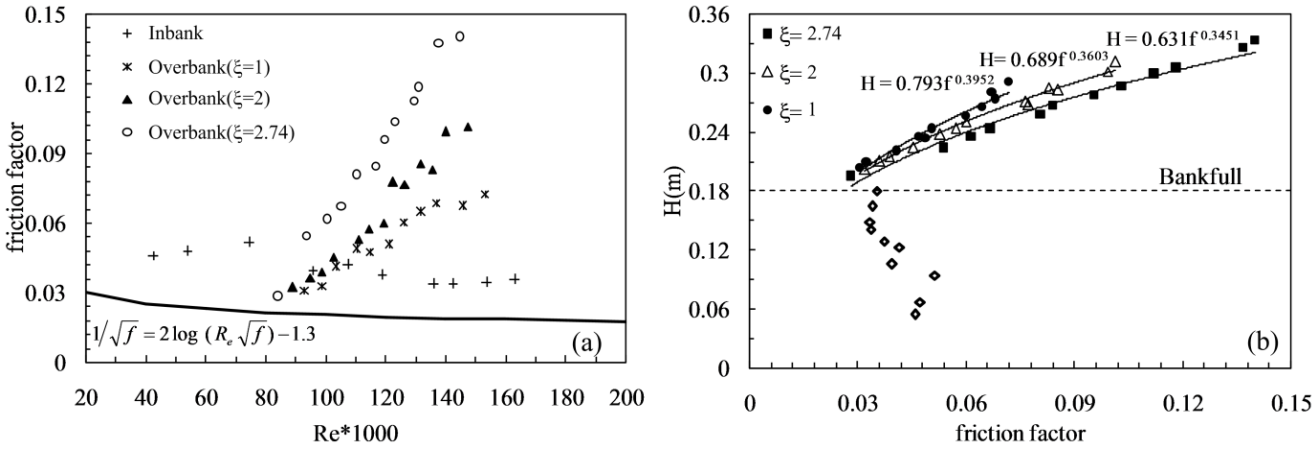

Figure18. Changes the overall friction factor in prismatic compound channel versus (a) Reynolds number (b) flow depth

The changes of the zonal and local friction factor for the test denoting NP-11.3°–ξ-0.15 was plotted in Figure 19. This Figure shows that when the roughness ratio increases, the values of the friction factor increase. Also, at the middle of divergence area, the values of zonal and local friction factor approximately were equal but at the end of that area, the values of local friction factor always were less than the values of zonal friction factor. This may be due to the effects of the secondary current in panels on floodplain surface and near the interface line.

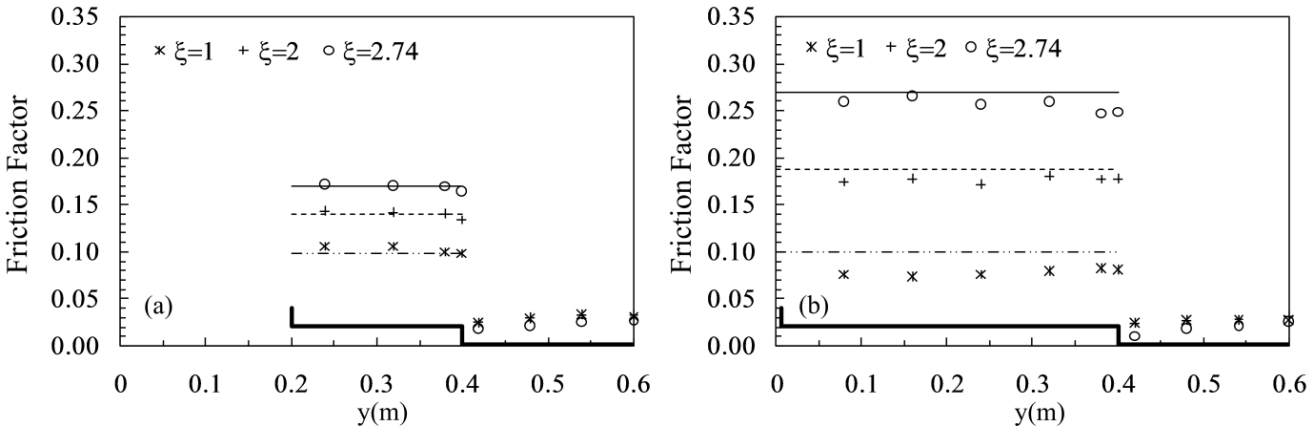

Figure 19. Comparison between local and zonal friction factor (a) NP-11.3°–ξ –0.15 (b). NP-11.3°-ξ -0.15 at middle and end of divergence reach respectively

In addition, the values of zonal friction factor in the main channel were a good agreement with equation below (Abril and Knight 2004):

$$f_{mc} = 8\left[5.75 \times \log\left(\frac{4H}{d}\right)\right]^{-2} \quad (15)$$

In which, d = bed material size (m).

Shear stress

Based on the above conditions for velocity profiles, after calculating the shear velocity, the shear stress at all of the panels (Figure 3) was estimated. Using the SKM and modified SKM, shear stress values also were calculated.

Figure 20 shows the lateral changes of shear stress with the SKM and modified SKM which were calculated in experiments. The modified SKM was due to the ability to accurately estimate the lateral depth-averaged velocity which can be set properly to the shear stress.

The gradient shear stress (ψ) at the interface zone in tests NP-11.3-ξ-D_r is shown in Figure 21. As seen, with an increase in the roughness on the floodplain surface, the difference between the velocity in the main channel and floodplain increased. Then, the gradient shear stress at this area was increased. Furthermore, at the interface zone, the rate of shear stress changes at the middle of divergence area was more than the end.

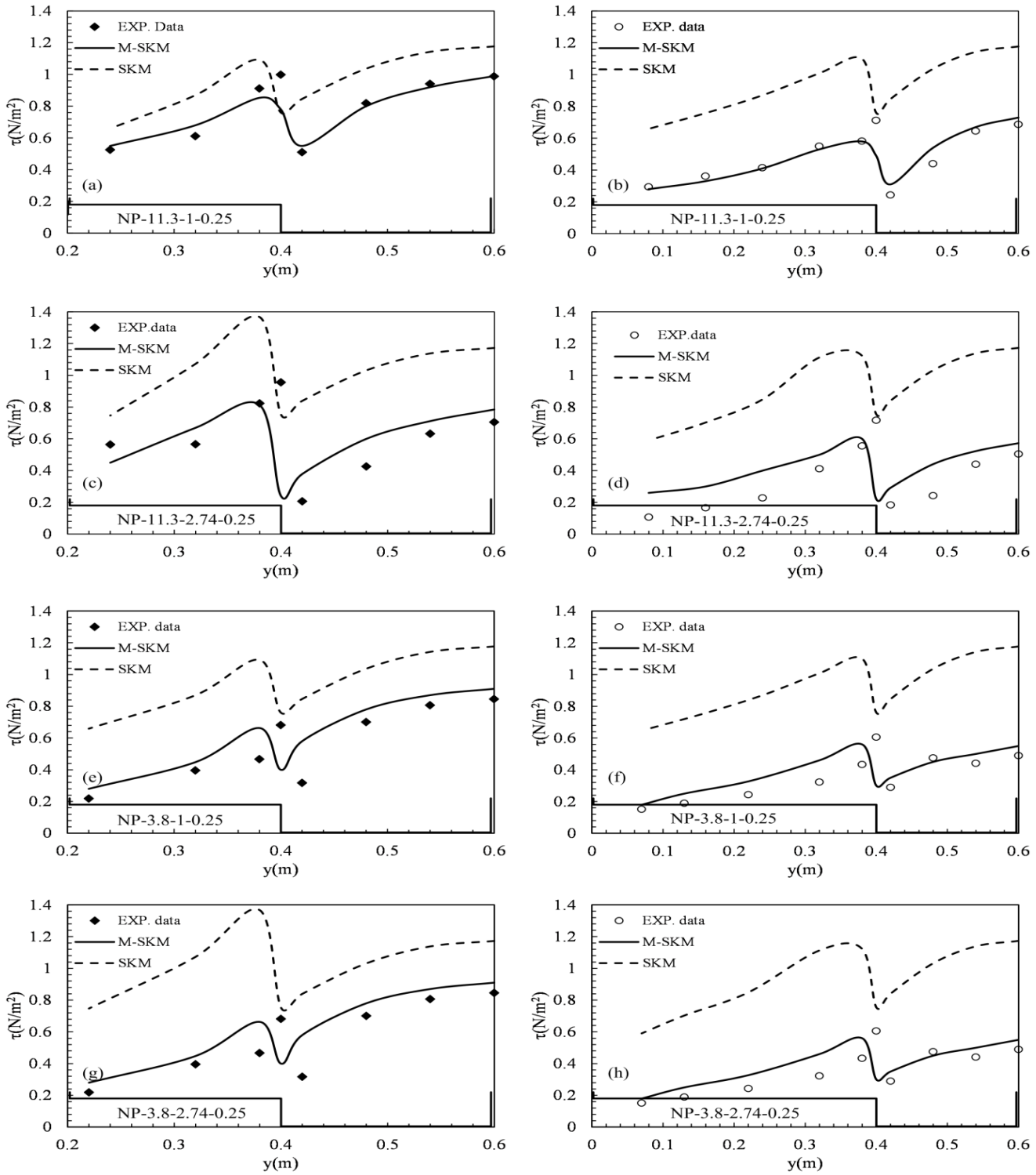

Figure 20. Comparison between shear stress in tests data with the SKM and modified SKM
(a, b) NP-11.3-1-0.25 (c, d) NP-11.3-2.74-0.25 (e, f) NP-3.8-1-0.25 (g, h) NP-3.8-2.74-0.25 at the middle and end of divergence reach respectively

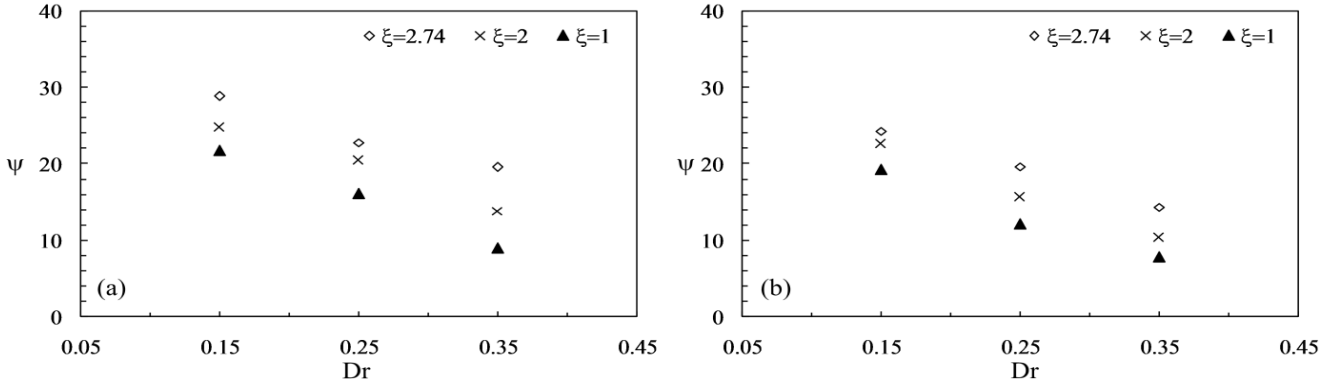

Figure 21. Gradient of shear stress at interface zone (a) Middle (b) End of divergence area in tests NP-11.3-ξ -D_r

Secondary flow term changes and turbulence intensities

In the experiments with the depth ratio equal 0.35, the values of the secondary flow term $\left[\Gamma = \frac{\partial}{\partial y}\left(H(\rho UV)_d\right)\right]$ and the Reynolds shear stress at three sections (entrance, middle and end of divergence) were measured by using ADV data. The changes of Γ in the tests of P-ξ-0.35 and NP-3.8–1–0.35 are shown in Figure 22, a maximum value that occurs at near the interface zone.

Also with an increase in the roughness ratio, the values of this term near the interface increased. This subject was not only true for the non-prismatic shape but also at the middle of reach was very high.

The turbulence intensities $(u'^2/u_*^2, v'^2/u_*^2)$ at middle and end of divergence reach are plotted in Figure 23. Results show that at the middle of divergence angle, turbulence intensity is much higher than that in the end of divergence area. With an increase in the roughness ratio, angle of divergence and decreasing depth ratio, the values of turbulence increases.

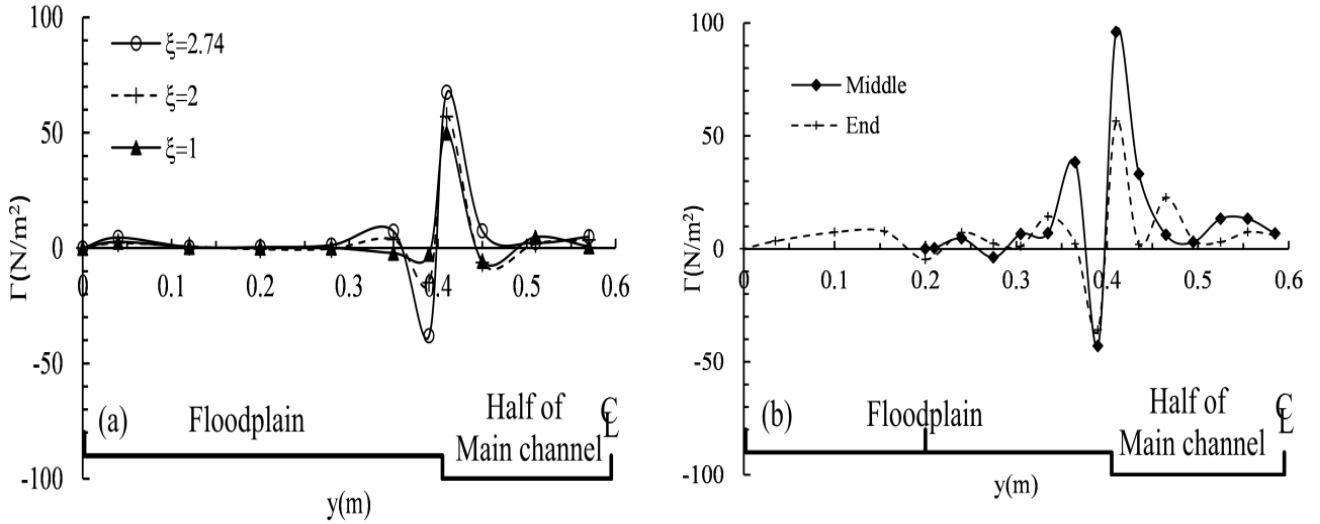

Figure 22. Lateral distribution of Secondary flow term in test (a) P-ξ-0.35 (b) NP-3.8-1-0.35

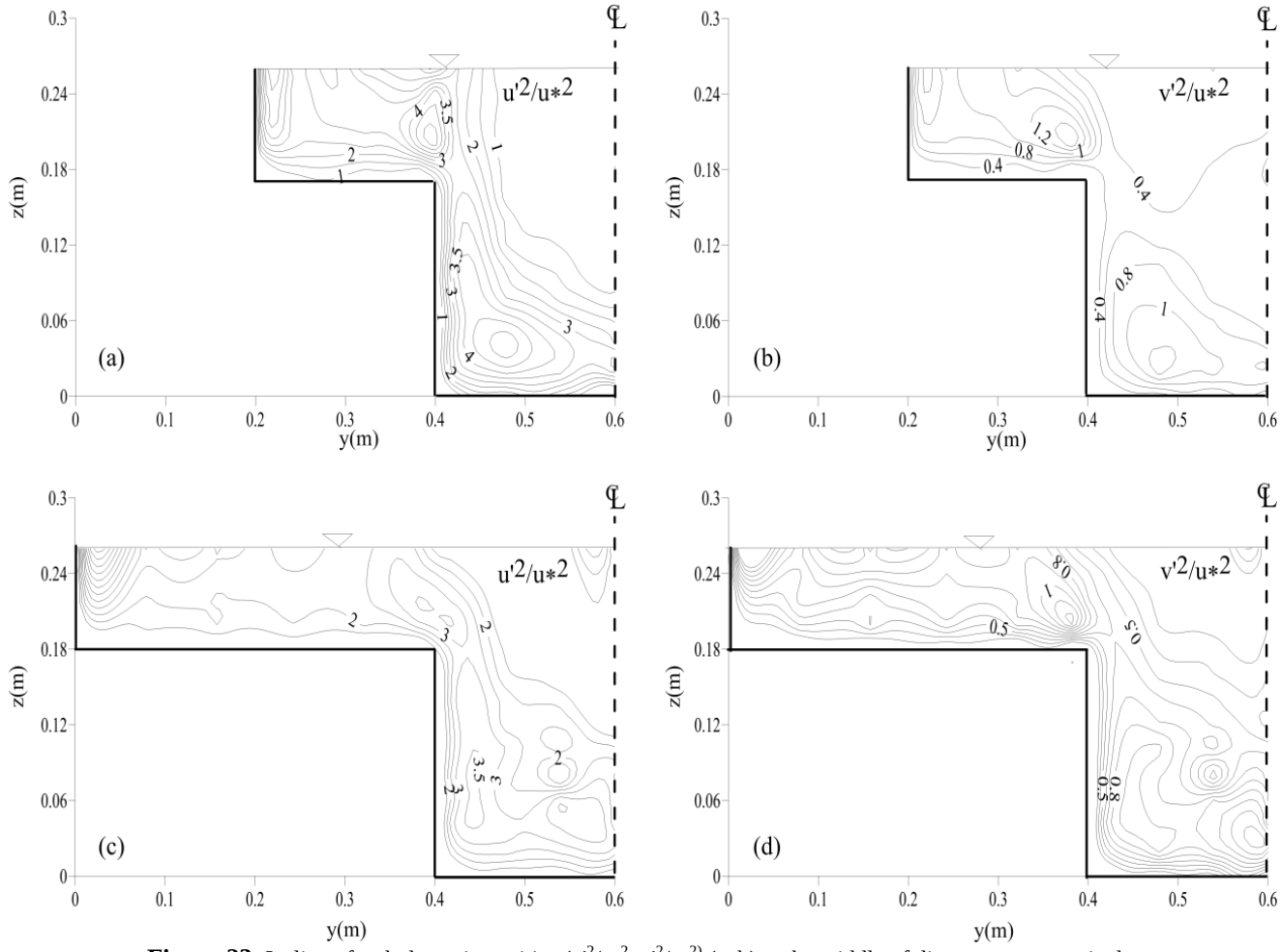

Figure 23. Isoline of turbulence intensities (u'^2/u_*^2, v'^2/u_*^2) (a, b) at the middle of divergence respectively (c, d) at end of the divergence area in test NP-11.3-2.74 -0.35

Comparison between the results of experiment and the SKM and Modified SKM

Based on depth-averaged velocity measurement and results of the SKM and modified SKM, the discharges, were calculated. The results show that with an increase in the depth ratio or decrease in the divergence angle, the discrepancy between the discharges measured and obtained from the SKM and Modified SKM decreased. The relative overall discharge error (%Q_e) in NP-3.8-ξ-0.15, 0.35 and NP-11.3-ξ-0.15, 0.35 at two selected section (middle and end of divergence reach) are shown in Figure 24.

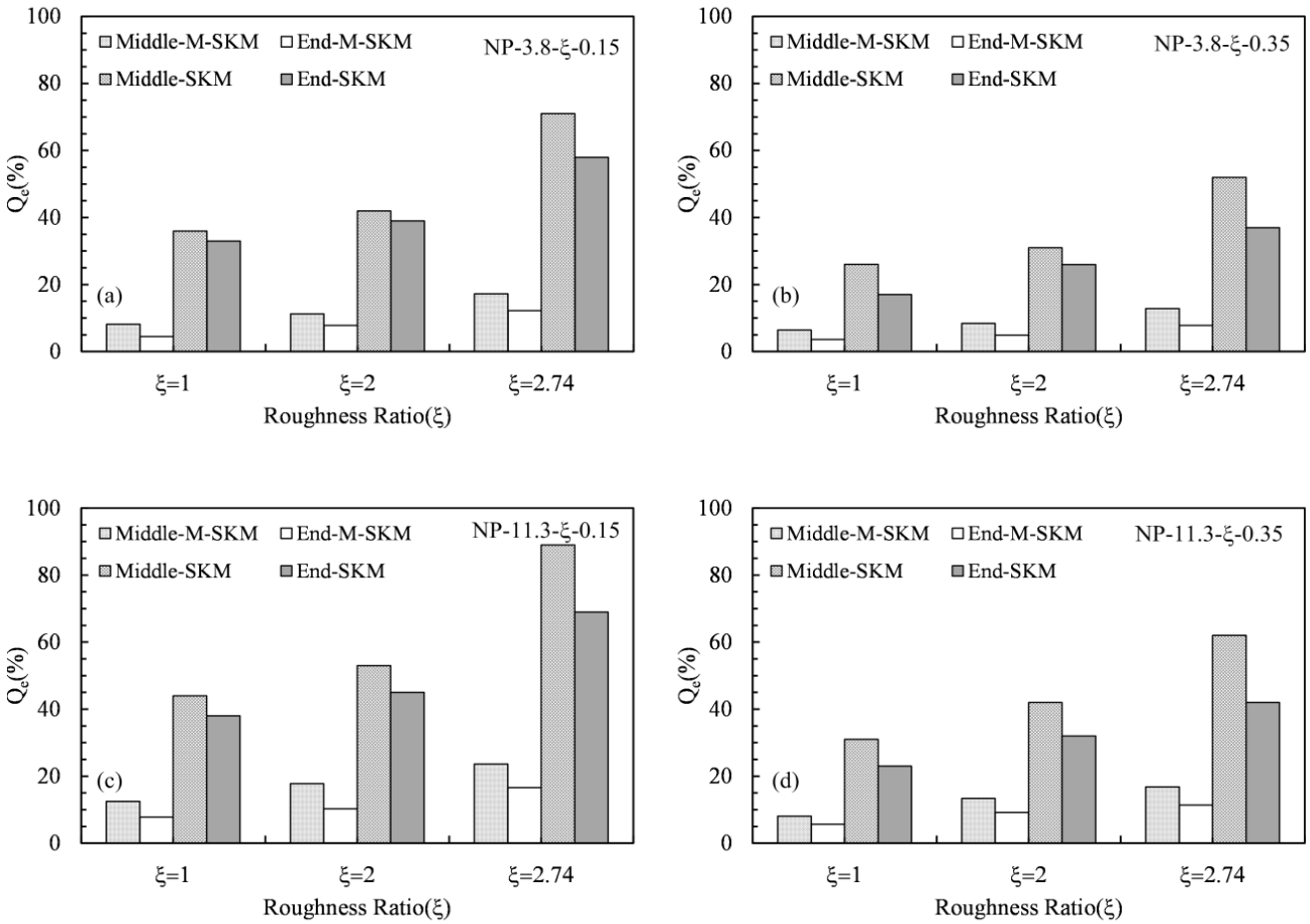

Figure 24. Relative overall discharge error (%Q_e) from the SKM and modified-SKM with experiment data (a, b) NP-3.8–ξ-0.15, 0.35 (c, d) NP-11.3-ξ-0.15, 0.35

CONCLUSION

The results of the current research were concerned with the velocity distribution, percentage divided discharge, friction factor, shear stress, secondary flow, and turbulence intensities in the non-prismatic compound channel with various roughnesses on the floodplain and three angles of divergence at flood plain (3.8^o, 5.7^o and 11.3^o).

Also the experiments data were compared with results of the SKM and modified SKM.

The most important results are summarized as follow:

By increasing the depth ratio or decreasing roughness ratio the velocity gradient between main channel and floodplain at middle and end of divergence reach decreased.

Increasing angle of divergence led to an increase in the gradient of velocity. Percentage divided discharge directly was impressed by roughness ratio and depth ratio.With an increase in the roughness on floodplain surface, the shear stress gradient increased.

Most of the changes of secondary flow term and turbulence intensities occurred at near the interface zone and at middle of the reach of those parameters which larger than were end of divergence reach.

Finally, comparison of the results of the SKM and modified SKM with the experiments' data show that firstly, the bed slope was not suitable for prediction of velocity and shear stress. But the use of the energy line slope, the flow conditions in model entirely looked like the experiment conditions. Secondly, with an increase in the roughness on the floodplain surface, the accuracy of the SKM and M-SKM decreased.

REFERENCES

1. Abril JB and Knight DW (2004). Stage-discharge prediction for rivers in flood applying a depth-averaged model. Journal of Hydraulic Research, 42(6): 616-629.
2. Ackers P (1991). Hydraulic design of straight compound channels. Report SR 281, Hydraulics Research Ltd Wallingford, England.

3. Bousmar D and Zech Y (2004). Velocity distribution in non-prismatic compound channels. Water Management, 157(WM2): 99-108.
4. Bousmar D, Proust S and Zech Y (2006). Experiments on the flow in a enlarging compound channel. Procceding River Flow, Lisbon, Portugal, (1): 323-332.
5. Cao Z, Meng J, Pender G and Wallis S (2006). Flow Resistance and Momentum Flux in Compound Open Channels. Journal of Hydraulic Engineering, 132(12): 1272-1282.
6. Hu C, Ji Z and Guo Q (2010). Flow movement and sediment transport in compound channels. Journal of Hydraulic Research, 48(1): 23-32.
7. Knight DW and Demetriou JD (1983). Flood plain and main channel flow interaction. Journal of Hydraulic Engineering, 109(8): 1073-1092.
8. Knight DW and Hamed ME (1983). Boundary shear in symmetrical compound channels. Journal of Hydraulic Engineering, 110(10): 1412-1430.
9. Knight DW and Tang X (2008). Zonal discharges and boundary shear in prismatic channels. Institution of Civil Engineers, 161(EM2): 59.68.
10. Myers WRC (1987). Velocity and discharge in compound channels. Journal of Hydraulic Engineering, 113(6): 753-766.
11. Proust S, Bousmar D, Rivière N, Paquier A and Zech Y (2010). Energy losses in compound open channels. Advances in Water Resources, 33: 1-16.
12. Proust S, Rivière N, Bousmar D, Paquier A, Zech Y and Morel R (2006). Flow in Compound Channel with Abrupt Floodplain Contraction. Journal of Hydraulic Engineering, 132(9): 958-970.
13. Rezaei B and Knight DW (2009). Application of the Shiono and Knight Method in compound channels with non-prismatic floodplains. Journal of Hydraulic Research, 47(6): 716–726.
14. Rezaei B and Knight DW (2011). Overbank Flow in Compound Channels with Non-prismatic Floodplains. Journal of Hydraulic Engineering, 137(8): 815-824.
15. Smart GM (1999). Turbulent velocity profiles and boundary shear in gravel bed rivers. Journal of Hydraulic Engineering, 125(2): 106-116.
16. Shiono K and Knight DW (1991) Turbulent Open channel flows with variable depth across the channel. Journal of Fluid Mechanics, 222: 617-646.
17. Tominaga A and Nezu I (1991). Turbulent structure in compound open-channel flows. Journal of Hydraulic Engineering, 117(1): 21-41.
18. Tang X and Knight DW (2009). Analytical models for velocity distributions in open channel flows. Journal of Hydraulic Research, 47(4): 418-428.